LASER INTERFEROMETER GRAVITATIONAL WAVE OBSERVATORY
- LIGO -
CALIFORNIA INSTITUTE OF TECHNOLOGY
MASSACHUSETTS INSTITUTE OF TECHNOLOGY

Technical Note	**LIGO-T1800201–v2**	2018/09/28

Developing Phase Map of Cavity Mirrors using Laser Mode Spectroscopy

Final Report - SURF 2018

Keerthana S Nair
Mentors: Koji Arai, Gautam Venugopal and Rana Adhikari

California Institute of Technology
LIGO Project, MS 18-34
Pasadena, CA 91125
Phone (626) 395-2129
Fax (626) 304-9834
E-mail: info@ligo.caltech.edu

Massachusetts Institute of Technology
LIGO Project, Room NW22-295
Cambridge, MA 02139
Phone (617) 253-4824
Fax (617) 253-7014
E-mail: info@ligo.mit.edu

LIGO Hanford Observatory
Route 10, Mile Marker 2
Richland, WA 99352
Phone (509) 372-8106
Fax (509) 372-8137
E-mail: info@ligo.caltech.edu

LIGO Livingston Observatory
19100 LIGO Lane
Livingston, LA 70754
Phone (225) 686-3100
Fax (225) 686-7189
E-mail: info@ligo.caltech.edu

http://www.ligo.caltech.edu/

1 Abstract

The LIGO gravitational wave detectors are special type of Michelson Interferometer with Fabry-Perot cavity introduced to it. In advanced LIGO, the arm lengths of the interferometers are 4 Km each. But this project is conducted in the LIGO-40m prototype, whose arm length is 40 m each. Each arm of the interferometer is capped with semi transparent mirrors through which the laser light gets transmitted and reflected. Any imperfection on the surface of these mirrors can result in optical power losses in the cavity. If the cavity mirrors are spherical, the modes of the Gaussian beam will resonate at frequencies which are equally spaced between each other. But in real, the mirrors are not exactly spherical. The mirror surface contains some imperfections which we call as the figure error of the mirror. These mirror figure errors cause the resonant frequencies of different higher order modes to shift from the ideal position. The aim of this project is to use interferometric technique to measure the deviation in resonant frequency spacing of such modes and to understand the figure error present on the mirror surfaces.

2 Introduction

The existence of gravitational wave was predicted by Albert Einstein in 1916 with the help of his general theory of relativity. According to Einsteins relativity presence of mass or energy bends the spacetime and accelerating massive objects like neutron star or blackholes produce time varying ripples in the spacetime. These ripples are known as the Gravitational Waves[1]. These waves would travel at the speed of light through the Universe. Study of these waves will give us information about the origin of these waves, nature of gravity and also a better picture of the universe.

The Laser Interferometer Gravitational Wave Observatory (LIGO) is a large-scale physics experiment and observatory to detect cosmic gravitational waves. It works with the help of two detectors located in Livingston, Louisiana and in Hanford, Washington. The first direct detection of Gravitational Waves was done by LIGO on September 14, 2015 [2]. This work earned three scientist the 2017 Nobel Prize in Physics.

The interferometers work on the principle of merging of two or more EM waves by a laser to create an interference pattern, which contain information about the object or phenomenon influencing it. This technique can be used to make extremely small measurements that are not achievable using other techniques. The detector used in LIGO is a modified Michelson interferometer with Fabry-Perot cavities introduced to it as shown in Figure 1. This modified Michelson interferometer has a L shape, in which each arms are of 4 km length. Each arm of the detector forms a Fabry-Perot cavity capped by a semi-transparent Input Test Mass (ITM) and an End Test Mass (ETM) [3].

Assuming that the suspended mirrors of the interferometer are still, the returning beam from each arm has a constant relative phase in the absence of gravitational waves. Thus, the

interference condition of the Michelson interferometer is stationary. When a gravitational wave passes through the detector it changes the differential of the arms by making it contract or expand. Now, the intensity of the TEM_{00} mode obtained at the output port will be different from the one we obtained when both the arms were of same length. Thus, these interference patterns can be used to make the precise measurement of the change in length occurred and also the nature of gravitational waves causing this change.

The change in length of the interferometer arm caused by the gravitational wave is about 10^{-19} m. Measurements of this scale is done by increasing the interaction time of Gravitational Waves with each arm. This is done by introducing a Fabry-Perot cavity inside each arm in which, laser beam effectively undergoes multiple reflections. But this increases the chance of power loss due to unwanted scattering from the mirror surfaces (ITM and ETM). The scattering can be due to point defects, scratches, sleeks, contaminations and Figure error of the mirrors [5]. The aim of this project is to precisely characterize the figure error of an optical cavity using an interferometric measurement. If we can reduce the power loss efficiently, it will help us to operate the interferometers with increased power efficiency and reduced scattered light problem.

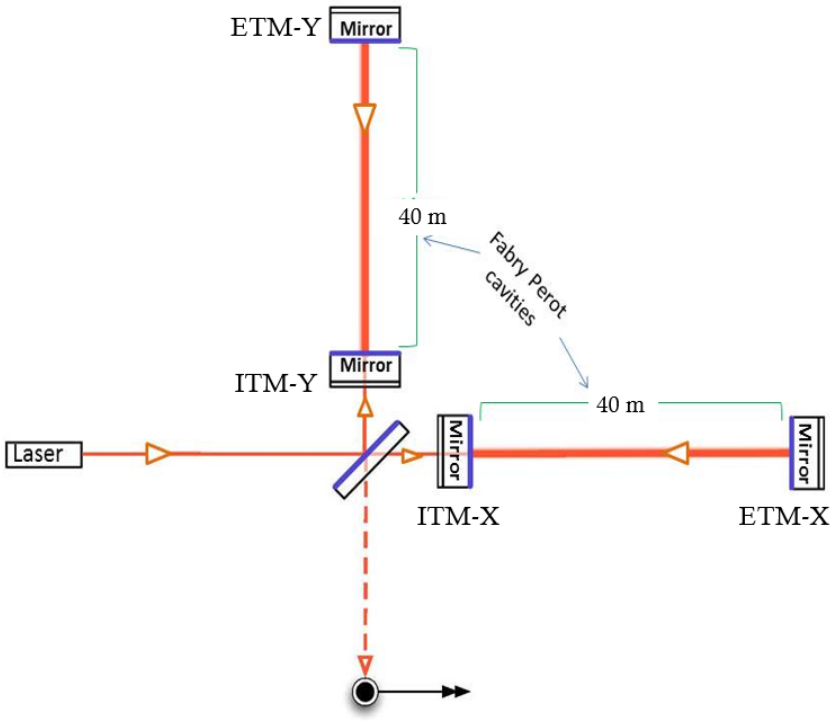

Figure 1: Schematic diagram of the LIGO 40m interferometer [4].

3 Objectives

The objectives of this project are listed below.

1. Using Finesse software for obtaining the ideal cavity scan data and estimating the free spectral range and transverse mode spacing corresponding to a particular frequency scan.

2. Obtaining the cavity scan data from the experiment and comparing these experimental deviations with theoretical mode spacings.

3. By analysing this data, precisely characterizing the figure error of an optical cavity by plotting Phase Maps.

Mirror figure errors are the low frequency surface defects present on the test masses which results in the low angle scattering of the light. This causes power loss in the optical cavities, which ultimately leads to destruction of squeezed state of light. Also, the classical couplings of the scattered light degrades the sensitivity of the interferometer. Through this project we are trying to develop a in-situ technique to precisely characterizing the figure error of an optical cavity.

Mirror figure error can be characterised by using Phase Maps. Phase Maps are those diagrams that show us the imperfections in the surface of mirror which contribute towards the power loss through scattering. The conventional technique to create these mirror map is Fizeau interferometry. But this cannot be done inside the LIGO interferometer without pulling the optic out of the interferometer. Thus, we are interested in developing a technique which can be used in the LIGO interferometer. Such techniques are classified as In-situ measurement techniques.

4 Approach

4.1 Optical Resonator

An optical resonator is a system containing two mirrors (ITM and ETM) separated by a distance. The Fabry-Perot cavity introduced in the Michelson interferometer act as an optical resonator. The laser beam passing through each arm bounces back and forth between the mirrors, which leads to power recycling. Optical resonators are characterised by the radius of curvature of the mirrors and the absolute distance between them.

An optical resonator has a certain set of modes which are allowed to resonate inside it. All the modes obtained in the transmission spectrum of the Fabry-Perot Michelson Interferometer can be expressed as a linear combination of these cavity eigen modes. The Hermite-Gaussian plynomials form a basis onto which all the modes for an ideal FP cavity can be projected. The resonance happens at different laser frequencies for different cavity eigen modes. An image of the intensity distribution corresponding to different Hermite-Gaussian modes obtained from the transmission spectra is shown in Figure 2. The cavity has repetitive resonances with the laser frequency. The spacing between two adjacent such modes are known as the Free Spectral Range (FSR) [8]. The free spectral range frequency (ν_{FSR}) is defined as,

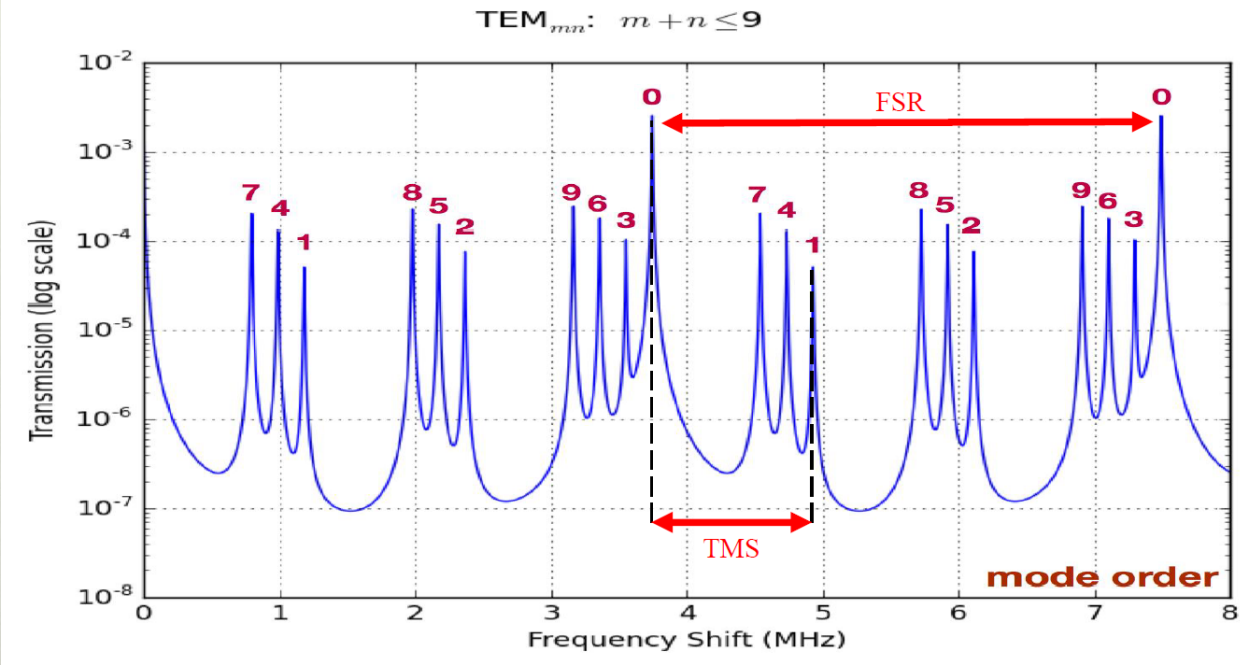

Figure 2: Intensity distribution corresponding to different Hermite-Gaussian modes obtained from the end transmission of each arm. The Fee spectral range and Transverse mode spacings are marked in this graph [7].

$$\nu_{FSR} = \frac{c}{2L} = 3.7474 \times 10^6 \text{ Hz}$$

Here, c is the speed of light and L is the length of the cavity which is equal to 40 m. These resonances are known as the fundamental mode resonance. Apart from these fundamental mode resonances in the transmission spectrum, there are higher order Transverse mode resonances. The distance between fundamental mode resonance and higher order Transverse mode resonance is known as the Transverse mode spacing (ν_{TMS}). For TEM$_{nm}$ mode, transverse mode spacing will be equal to,

$$\nu_{TMS} = \nu_{FSR} \left(\frac{n+m}{\pi}\right) \cos^{-1} \sqrt{g_1 g_2}$$

The g-parameter for this cavity are given by,

$$g_1 = 1 - \frac{L}{R_1} \approx 1$$
$$g_2 = 1 - \frac{L}{R_2} \approx 0.298$$

Here $R_1 = \infty$ and $R_2 = 60$ m are the radius of curvature of the ITM and ETM mirrors. Then for a TEM$_{nm}$ mode, the ν_{TMS} will be equal to

$$\nu_{TMS} = (n+m)1.14 \times 10^6 \text{ Hz}$$

The Gouy phase shift of the beam, $\phi(z)$ is defined as,

$$\phi(z) = \arctan\left(\frac{z}{z_R}\right)$$

where, z_R is the Rayleigh range, or the distance along the z-axis at which the wavefronts of the beam are most curved,

$$z_R = \frac{\pi {W_0}^2}{\lambda}$$

We can also write ν_{TMS} as,

$$\nu_{TMS} = \nu_{FSR}\left(\frac{n+m}{\pi}\right)\Delta\phi$$

where $\Delta\phi$ is the total Guoy phase shift of the cavity defined as,

$$\Delta\phi = \phi(z_1) \text{ - } \phi(z_2) = \cos^{-1}\sqrt{g_1 g_2}$$

We can thus write the resonance frequencies of the general spherical-mirror cavity mode as

$$\nu_{lmq} = \mathrm{q}\nu_{FSR} + \left(\frac{n+m+1}{\pi}\right)\nu_{FSR}\,\Delta\phi$$

where q is an integer indicating the longitudinal mode number.

The different longitudinal modes of the cavity are those with the same values of (n,m) but different values of q. As in the Fabry-Perot cavity, adjacent resonant frequencies are separated by ν_{FSR}; thus, the longitudinal mode spacing is determined by the absolute length of the cavity.

Different transverse modes are determined by the indices (n, m), which indicate spatial dependencies along the x and y axes, respectively. Adjacent transverse modes with indices (n_1, m_1) and (n_2, m_2), of the longitudinal mode q [9], are spaced by

$$\nu_{(n_1,m_1,q_1)} \text{ - } \nu_{(n_2,m_2,q_2)} = [(n_1 + m_1) \text{ - } (n_2 + m_2)]\,\frac{\nu_{FSR}\Delta\phi}{\pi}$$

apart. Thus, the spacing of the transverse modes of a cavity depends on the radius of curvature of the cavity mirrors. The intensity distributions of several of the low-order transverse Hermite-Gaussian modes are shown in Figure .

4.2 Frequency shift for higher order modes

For a given transmission spectrum we can find both ν_{FSR} (Free Spectral Range), the spacing between adjacent fundamental modes and ν_{TMS} (Transverse mode spacing), the difference in frequency between a higher-order mode peak and the fundamental mode peak. We have already discussed how to find ν_{FSR} and ν_{TMS} in the case of perfectly spherical mirror. But in the real case scenario, the mirrors are not perfectly spherical. The imperfections or the

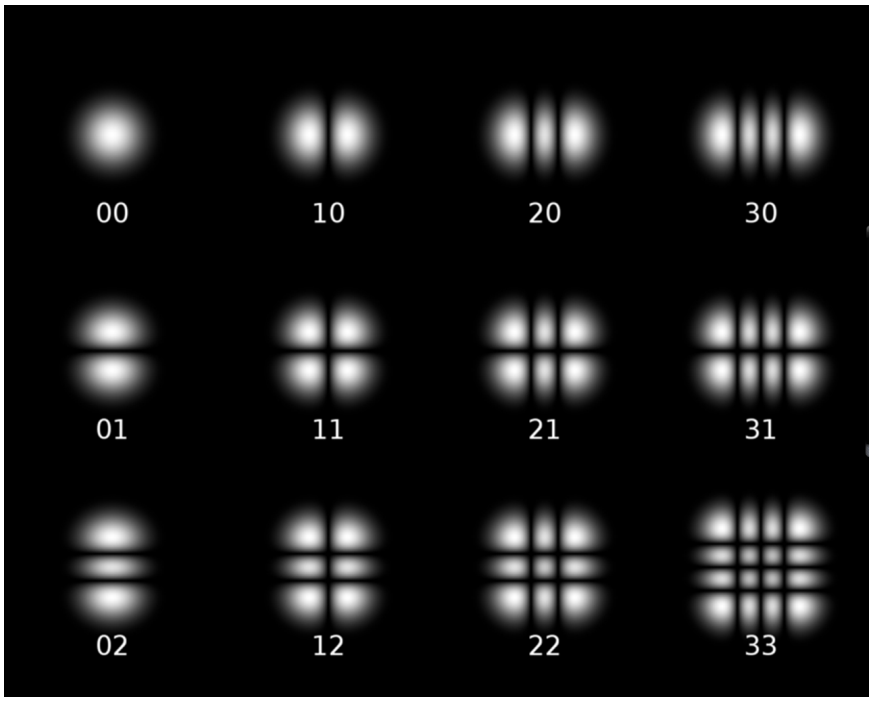

Figure 3: Intensity distributions of several transverse Hermite-Gaussian modes. The indices (n,m) are labeled beneath each mode. We can see that the intensity distribution of the mode with indices (n, m) has n nodes along the horizontal direction and m nodes along the vertical direction [7].

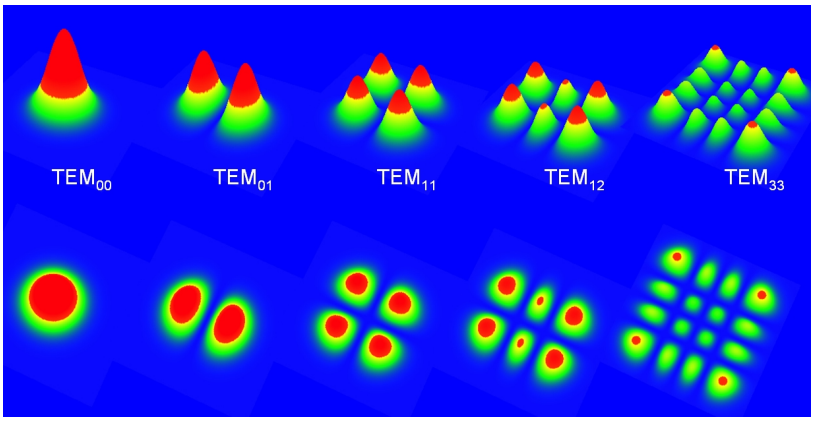

Figure 4: 3-D intensity distributions of several transverse Hermite-Gaussian modes [10].

figure error present on the mirror surface causes the mode frequency of the higher order modes to shift from its expected positions.

The frequency of each of the mode gets affected differently depending on the property of the mirror surface, each mode comes in contact with. As we have seen before in the last section, ν_{TMS} should vary linearly with Hermite-Gaussian mode order.

$$\nu_{TMS} = \nu_{FSR} \left(\frac{n+m}{\pi}\right) \cos^{-1} \sqrt{(1 - \frac{L}{R_1})(1 - \frac{L}{R_2})}$$

Here $R_1 = \infty$. So,

$$\nu_{TMS} = \nu_{FSR} \left(\frac{n+m}{\pi}\right) \cos^{-1} \sqrt{(1 - \frac{L}{R_2})}$$

From this we see that a change in the radius of curvature of the ETM mirror, R_2 results in a change in ν_{TMS}. The radius of curvature of the region at which the mode comes in contact with the mode change the transverse mode spacing of that mode accordingly.

As an example, we can say that in case of TEM_{00} mode, it comes in contact with the centre of the mirror if the beam is perfectly aligned. Then the radius of curvature of the central region of the mirror decides the mode frequency.

Knowing this fact, we are trying to measure the shift in transverse mode spacing corresponding to each mode and using this information to find out the surface property of the mirror, which comes in contact with those regions. We are not calculating this directly using numeric. But we are going to use statistical analysis to find the perturbation which gives the most comparable result with the actual cavity scan data.

5 Experiential Technique

A schematic diagram of the interferometer we will be working on in this project is shown in Figure 1. We will be using scan data from only one arm of the interferometer. A simplified diagram of one arm of the interferometer is provided in Figure 5. Later this procedure can be done to the other arm in order to find out the Phase Map of the mirrors used in that arm. We are expecting the experimental scan data to look similar to that we predicted with the help of Finesse software. By analytical calculation we know the mode spacing corresponding to each mode. But the experimental scan data will show some shifts in frequency from the predicted frequencies. This shift is due to the presence of figure error in the mirrors used in the cavity. Thus, we introduce zernike polynomials into the Finesse simulation and apply phase map to the mirror. Bayesian inference can be used to find the phase map which best matches with the experimental data.

5.1 Frequency Scan

Neither the laser frequency nor the cavity length of the arms is stable enough to sustain the resonance of the cavity. Thus, we need to control either the laser frequency or the arm length

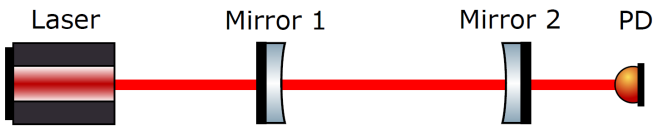

Figure 5: A simplified diagram of one arm of the interferometer [6].

to maintain the optical resonance. Thus, the main laser used in the interferometer is a pre-stabilised laser (PSL) whose frequency is locked to a particular value with the help of Pound Drever Hall Locking technique. For giving a scan to the frequency we cannot do any tuning to the main laser because of our inability to do this in a deterministic way. In order to give a scan to the frequency, we need to use some other techniques. Few of the techniques used by the previous students include cavity scan using Electric Optical Modulator (EOM), cavity scan using Additional Auxiliary Laser and Arm length stabilisation scheme. The method we are going to follow in this project to obtain the cavity scan is by using an Auxiliary laser. This process is known as the Phase locking. A schematic diagram of the Phase locking loop including the AUX laser is shown in Figure 6. The auxiliary laser beam is injected from an optical port, while the main laser is locked to one of the arm. This means that the PSL laser frequency is set in such a way that it resonates inside this cavity. But if the cavity length changes by a small amount, the PSL laser will adjust itself by varying the laser frequency to keep the laser locked. Thus, there exists an uncertainty in both the cavity length and also in the frequency of the PSL laser. But the feedback control ensures that the change in cavity length does not alter the locked condition of the PSL laser. The AUX and the PSL laser are connected through the PLL-loop (Phase Locked Loop). This loop ensures a constant phase difference between the PSL and AUX. Thus, it ensures a constant phase between the AUX and the cavity. This enables us to change the relative frequency of AUX and do the scanning process.

The electric field (E) of both PSL and AUX lasers are given below,

$$E_{PSL}(t) \approx \sqrt{P_{PSL}}\ e^{i\phi_{PSL}(t)}$$

$$E_{AUX}(t) \approx \sqrt{P_{AUX}}\ e^{i\phi_{AUX}(t)}$$

where P is the power of the laser and ϕ is the phase of the laser. These two fields undergo optical mixing to produce the beat note at the photo-detector (New Focus 1811).

$$P_{beat}(t) \approx \mid E_{PSL}(t) + E_{AUX}(t) \mid^2$$

$$P_{beat}(t) \approx P_{PSL} + P_{AUX} + 2\sqrt{P_{PSL}P_{AUX}}\ \cos\left[\phi_{PSL}(t) - \phi_{AUX}(t)\right]$$

The high-passed NF1811 beat readout signal from the photo-detector,

$$V_{PD}(t) \approx 2K_{PD}\ \sqrt{P_{PSL}P_{AUX}}\ \cos\left[\phi_{PSL}(t) - \phi_{AUX}(\mathrm{t})\right]$$

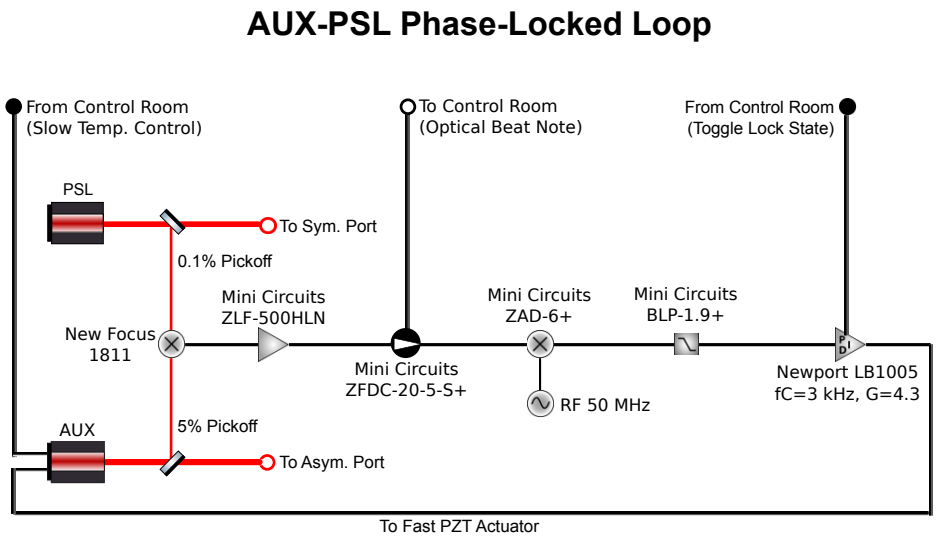

Figure 6: Schematic diagram of the AUX-PSL Phase locked loop

The RF-amplified readout signal is given by,

$$V_{amp}(t) \approx 2K_{amp}\ K_{PD}\ \sqrt{P_{PSL}P_{AUX}}\ \cos\ [\phi_{PSL}(t) - \phi_{AUX}(\mathrm{t})]$$

A part of this beat is taken to the control room with the help of coupler. This is connected to the frequency counter for getting the frequency display at each point of time. This display helps us to monitor the beat frequency when we want to engage the PLL to acquire the lock. If the beat frequency is far away from the frequency of the Local Oscillator (LO), we will not be able to acquire the lock of the PLL. The reason for this is that only for a limited range the mixer we use in the phase lock loop (PLL) will act as a linear mixer. Thus, we need to ensure that the relative frequency between AUX and PSL comes under this range before locking the loop. So, we need to observe the beat frequency and tune it by slowly adjusting the laser temperature. Once the beat frequency reach near the target frequency, the loop can be turned on and the lock can be acquired. We are providing an oscillatory frequency through the RF generator. The system will lock the two lasers in such a way that the frequency difference between PSL and AUX lasers remains a constant and this will be equal to the frequency provided by the RF frequency generator.

The RF gererator signal is given as,

$$V_{RF}(t) = V_{amp}\ \sin[\phi_{RF}(t)]$$

The beat signal and the RF signal passes through the mixer where it down convert beat signal to DC. Here the upper and the lower side bands are formed.

$$V_{mix}(t) = K_{mix}\ V_{amp}(t)\ V_{RF}(t)$$

$$= K_{mix}\ K_{amp}\ K_{PD}\ \sqrt{P_{PSL}P_{AUX}}\ V_{amp} \sin\left[\phi_{PSL}(t) + \phi_{AUX}(t) + \phi_{RF}(t)\right] \text{ (upper side band)}$$

$$- K_{mix}\ K_{amp}\ K_{PD}\ \sqrt{P_{PSL}P_{AUX}}\ V_{amp} \sin\left[\phi_{PSL}(t) - \phi_{AUX}(t) - \phi_{RF}(t)\right] \text{ (lower side band)}$$

The Low-Pass filter only allow the low frequency component to pass through and it eliminates the high frequency component. Thus the filter output is given as,

$$V_d(t) = -K_{mix}\ K_{amp}\ K_{PD}\ \sqrt{P_{PSL}P_{AUX}}\ V_{amp} \sin\left[\phi_{PSL}(t) - \phi_{AUX}(t) - \phi_{RF}(t)\right]$$

At lock point,

$$\phi_{AUX}(t) = \phi_{PSL}(t) - \phi_{RF}(t)$$

This signal pass through the PI control system (Proportional and Integration) and as a result feed back is given back to the fast frequency tuning of the AUX laser for adjusting its frequency in order keep the difference in frequency between PSL and AUX a constant.

5.2 Making the cavity scans

This stage involves aligning the interferometer, running the frequency scans and collecting the cavity scan data. There were many steps to be done in order to achieve this. The first task was making the code for setting and scanning the Marconi frequency, which act as the Local Oscillator in the phase locked loop. Also, the code needed to be command line enabled to ensure the smooth running. Python 2.7 is used to write all these codes. A picture of the MEDM control screen for locking the PLL is shown below in Figure 7. Instead of Marconi, an Agilent can also be used as the local oscillator. We have tried four different ways to produce the frequency scan. The first method is by scanning the AUX laser frequency using the Marconi. This directly changes the central frequency of the AUX laser. Second method is by providing RF frequency to the AOM. This sweeps the side band frequency of the AUX laser. Third one is the double demodulation technique. In this method, we use the Marconi and the Agilent together. Marconi act as the local oscillator and Agilent act as the RF generator. The signal from both these passes through a mixer and the output of this act as the local oscillator for the next stage. There, the photodiode output act as the RF generator and both these signals passes to the next mixer. A diagram of the double demodulation technique is shown in Figure 8. Fourth method is known as the single demodulation technique. In this the Agilent act as the local oscillator and photodiode output act as the RF generator. Diagram of this is shown in Figure 9.

5.3 Making the setup sensitive to the higher order modes

There are two ways to introduce higher order modes. One way is to introduce a slight misalignment between the PSL and the AUX beam which alters the gaussian nature of the beam and results in the higher order modes. Another way to do this is by introducing a

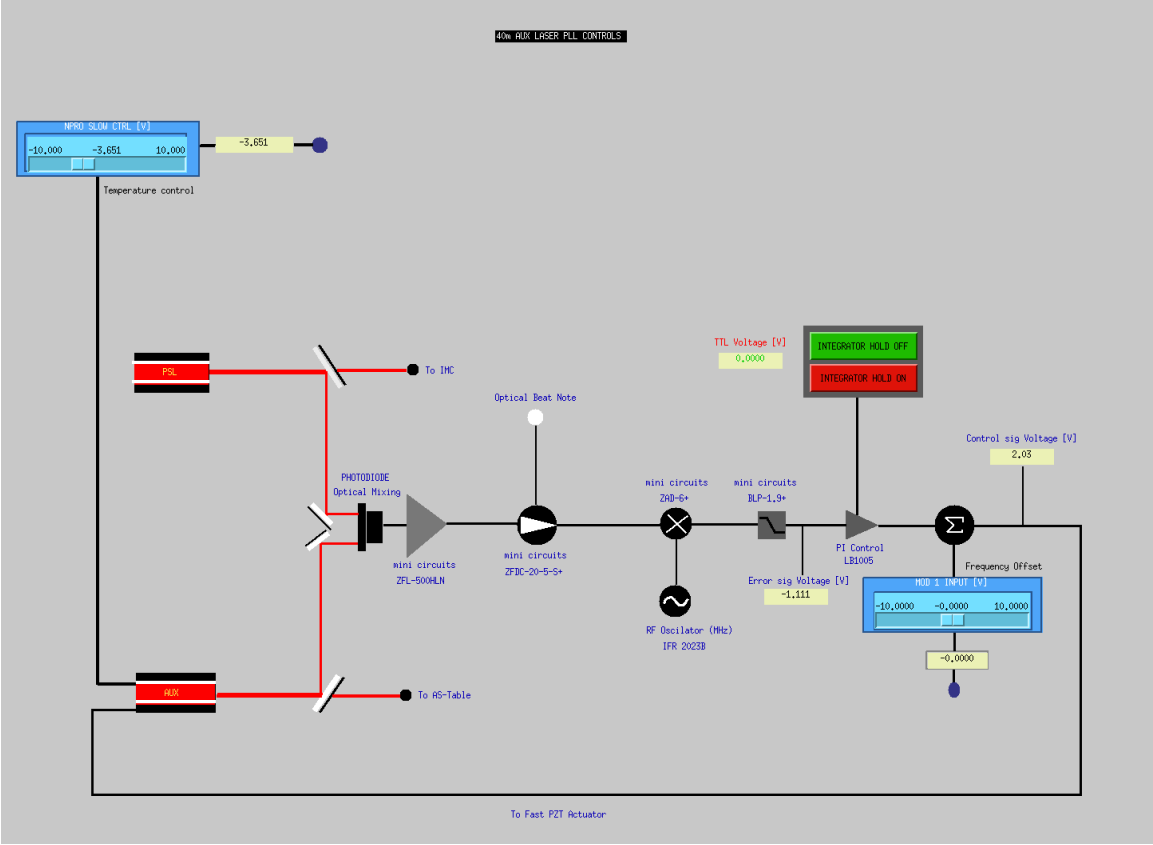

Figure 7: An image of the MEDM screen, used for controlling the AUX, PSL laser in order to achieve phase locking.

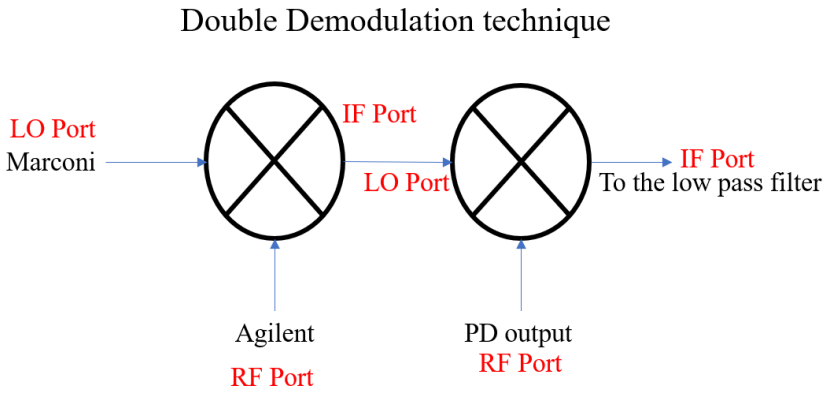

Figure 8: A schematic of the double demodulation technique. Here two mixers are used. The signal from the Marconi and that from the Agilent get mixed and the resultant signal get mixed with the PD output in the send mixer. The final signal goes to the low pass filter and from there the circuit is common for both single demodulation and double demodulation technique.

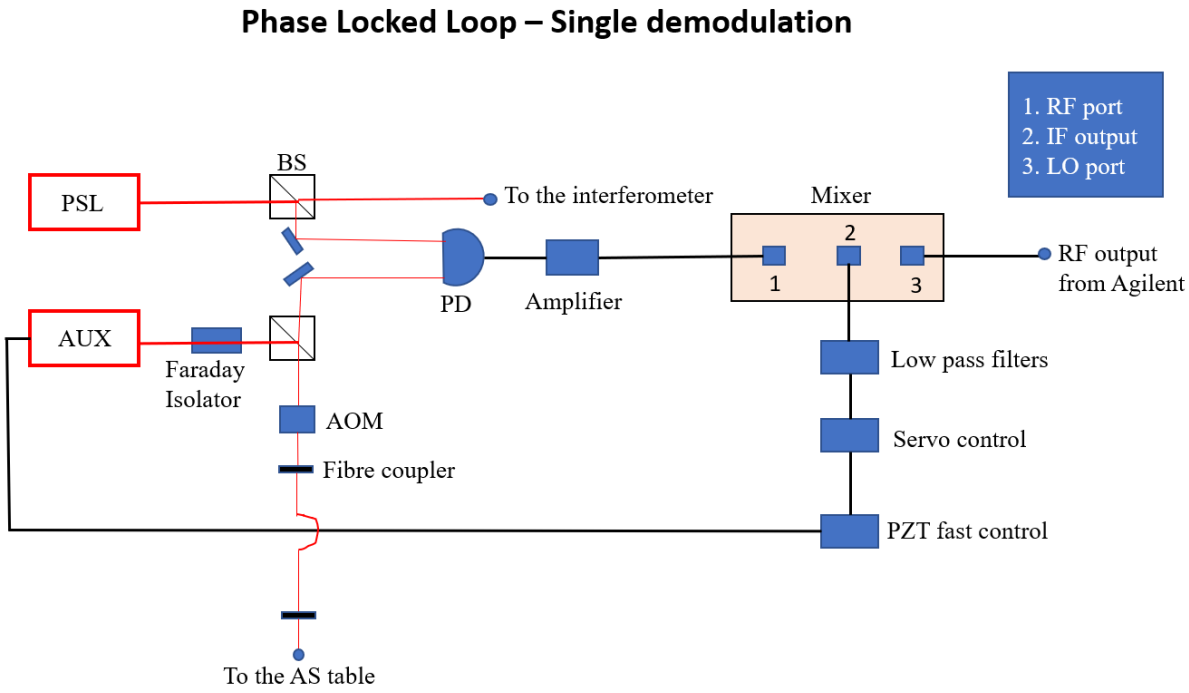

Figure 9: A schematic of the single demodulation technique. Here Marconi is not used and only Agilent is used.

sharp-edged object in front of the beam to alter its gaussian nature. As it took some effort to really align the cavity, we decided not to disturb the alignment and to try the second method. We tried this method by introducing a razor blade in the input and also in the output of the AUX beam. Inserting this in the input helps us to increase the power going to the higher order modes. And inserting the blade in the output helps us to take away its orthogonal property and prevent the higher order beam intensity cancelling out in the photodiode. We also replaced the razor blade by a thin two-prong fork and repeated the scan to see which method gives us better higher order mode content.

5.4 Obtaining the Phase data

Along with the amplitude data, we need to obtain the Phase data also. This phase data can be used to ensure the coherent nature of the measurement. We can use two methods for this purpose. One is by taking Marconi frequency as reference. This can be noisy because of the phase noise in the PSL beat setup. Another method to do this is by detecting beat note somewhere before the arm. For example, from the x-arm pick off. This will be helpful in the sense that this beat frequency will be exactly similar to the one which is going to the cavity from which we are collecting the data. Thus, the noise part can be reduced using this method.

5.5 Heating the ETM mirror

In order to get an estimate of change in Transverse mode spacing corresponding a particular figure error on the mirror, we introduced a known deformation on the mirror surface. The technique we used to create a known deformation on the mirror surface is by heating the mirror. The radiation energy emitted by the heater is focused at the centre of the ETM mirror with the help of lenses and Reflectors. This causes a deformation on the mirror surface as the heat energy makes the mirror surface to expand outwards. We used a rod heater for this purpose and we used two type of reflectors to see the heat pattern it forms at the mirror surface. They are cylindrical and elliptical reflectors. For testing it we made a setup using a cylindrical reflector as shown in Figure 10. An infrared image of the same setup is shown in Figure 11. The heat pattern produced by both the reflectors are different. Cylindrical reflector creates a heat pattern as shown in the Figure 12 and elliptical reflector creates a heat pattern as shown in the Figure 13.

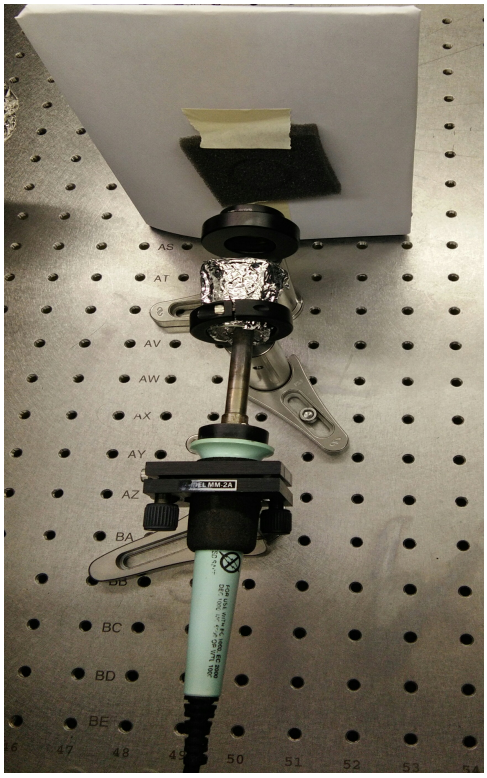

Figure 10: In order to design a suitable heater setup, for installing inside the ETM chamber we created this test alignment. Here a rod heater passes through a cylindrical reflector. With the help of a lens, we are trying to focus the radiation to the screen which is placed in front of the lens. Above the screen we have stacked a piece of sponge (for observing the heat imprints). The purpose of this test is to find out the heat pattern formed with the help of a cylindrical reflector.

In case of cylindrical reflector, the rod heater (30mm long, 3.8 mm diameter) is set inside the elliptical reflector, as close as possible to the first focus. The heater emits radiation all

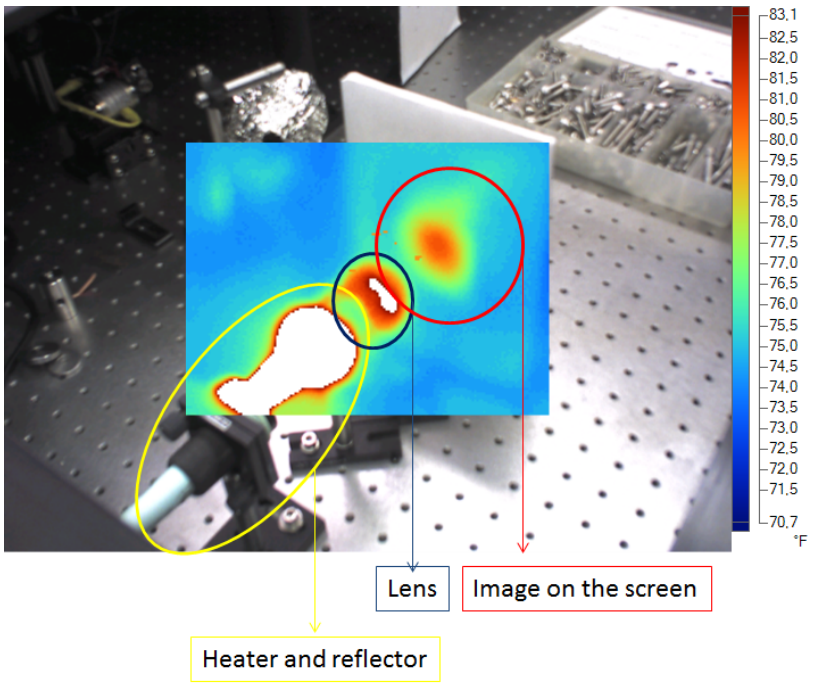

Figure 11: Infra-Red image of the test setup. This shows the temperature gradient present in different regions. The temperature scale corresponding to different colours are shown on one side of the image. From this we can clearly see the heat pattern formed from a cylindrical reflector.

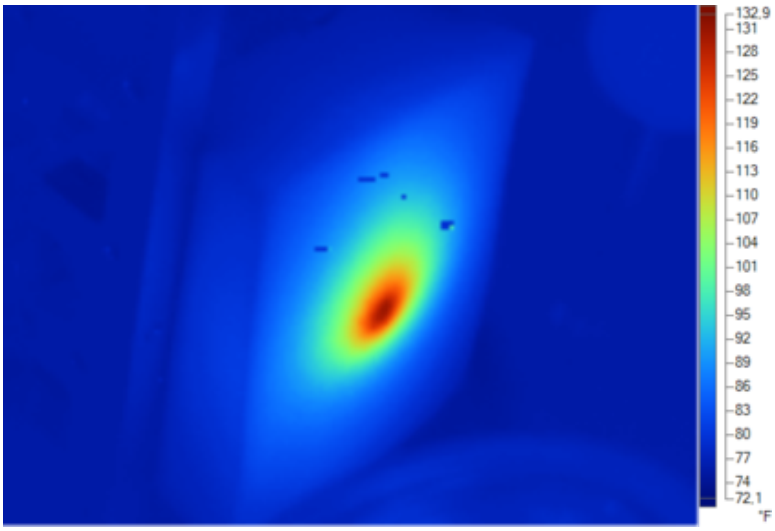

Figure 12: Zoomed in image of the heat pattern formed while using a cylindrical reflector. In this, the central region is having the highest temperature and as we move away from the centre, the temperature gradually decreases.

Figure 13: Representation of the heat pattern formed while using an elliptical reflector around the rod heater. In this, the central part is a local maximum. Then the temperature decreases till it reaches the next local maximum. A ring type structure of high temperature is formed with the help of this reflector.

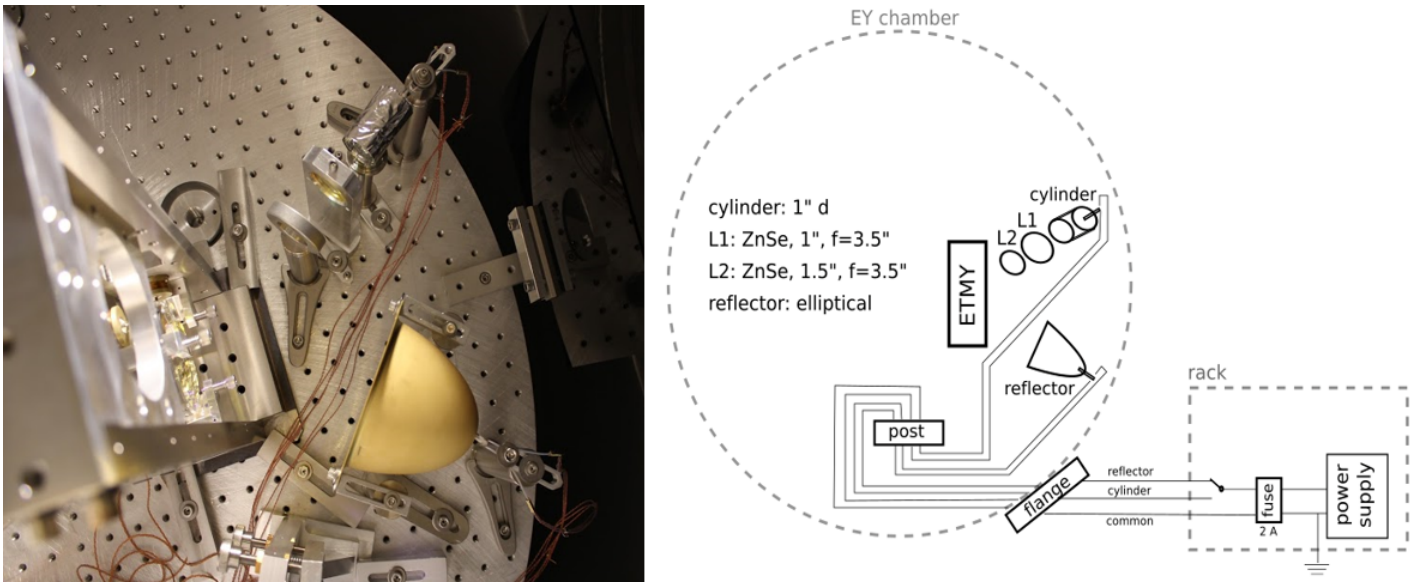

Figure 14: Image on the left side shows the real image of the heater setup inserted inside the ETM chamber. Whereas image on the right side shows the schematic diagram of the same. The parameters of all the components are also shown in the schematic.

over the spectrum with the Black Body radiation distribution, and the broadband power meter measures all of them, but only starting from 4 μm they will be actually absorbed by the mirror.

When the heat energy gets focused at the centre of the mirror, the mirror surface expands outwards. We can call this the thermal expansion of the mirror. This is because the rate of heat diffusion is less in case of glass and thus the excess energy given to the glass increases the energy of atoms inside this material. Thus, the material starts to expand outwards. Due to this expansion the curvature of the mirror reduces and this leads to a decrease in radius of curvature of the mirror. From the equation of ν_{TMS}, we know that a change in radius of curvature of the ETM mirror will create a change in the transverse mode spacing.

$$\nu_{TMS} = \nu_{FSR} \left(\frac{n+m}{\pi}\right) \cos^{-1} \sqrt{\left(1 - \frac{L}{R_2}\right)}$$

In this case R_2 is decreasing. This leads to an increase in the transverse mode spacing. So, after heating the ETM mirror we expect the ν_{TMS} to be greater than the same we get without heating. We already know that the deformity present on the mirror surface will affect each mode differently depending upon the point of contact. Thus, the shift present on each mode will also be different.

In order to test this prediction, we inserted a heater-reflector system near the ETM mirror. A diagram of the heater setup is shown in Figure 14. We have installed two rod heaters. One with elliptical reflector and one with cylindrical reflector. The heater system is inserted in such a way that it does not disturb the incoming laser signal. Having these two types of heater systems gives us freedom to analyse scan data from two or more type of known mirror figure errors.

6 Finesse Software

For extracting useful information from the cavity scan data, we need to have some idea about how the cavity scan data will look like and what should be expected as an output from this. For this purpose, we are using a software called Finesse. Finesse is a frequency domain interferometer simulation software developed by a team working in the GEO-600. This software is used to create interferometer simulations for designing and debugging the interferometers. We are using this software in this project to create simulations of the cavity scan data and to predict the output we are expecting from our interferometer setup. We are using Python to make the script and a package named PyKat is used to act as an interface between the Finesse software and the python. A flow chart useful for dealing this type of codes are shown in Figure 15. The parameters of the cavity which are needed for producing the ideal cavity scan is given below in the Table 1.

From the cavity scan data, the main data we are interested in extracting, is the central frequency corresponding to each peak (mode). For this, different fitting models are used. The one which I started with is the Least Square Fit. After that we would like to identify each peak and plot a graph of modes Vs the frequency. This graph is expected to be linear whose slope is equal to the free spectral range of the cavity. Fitting models can be prepared

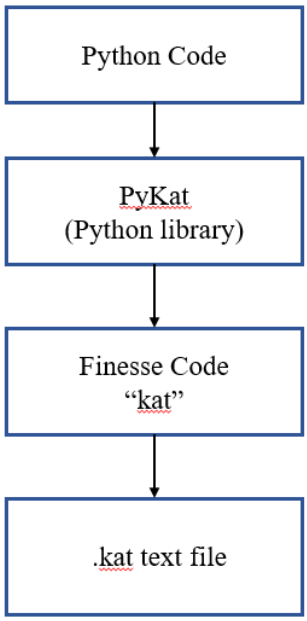

Figure 15: Flow chart showing the varous stages involved in producing a Finesse simulation.

Parameter	Value
Cavity length (L)	38.5 m
ITM Reflectivity (R)	0.98616
ITM Transmissivity (T)	0.01384
ETM Reflectivity (R)	0.9999863
ETM Transmissivity (T)	$1.37\text{x}10^{-6}$
ITM Radius of curvature (R_1)	∞
ETM Radius of curvature (R_2)	58 m

Table 1: Parameters of the 40m LIGO interferometer used for the Finesse simulation.

by using the finesse simulations and this model can be later implemented to the cavity scan data from the interferometer.

The schematic of the cavity which I used for simulating the cavity scan data is shown in Figure . In order to verify the consistency of Finesse solution comparing to the Analytical solution, both the graphs are plotted together as shown in Figure . The difference between both the results are found out and plotted as shown in Figure . The difference seems to be very much negligible and this shows that the Finesse solution is consistent.

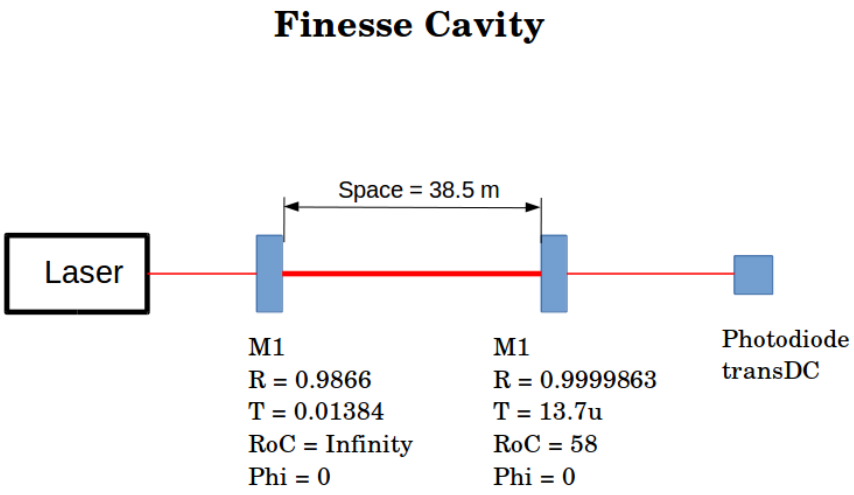

Figure 16: Cavity model used in finesse software for generating the ideal cavity scan data. The parameters corresponding to each component is mentioned below.

7 Analysing the cavity scan data

Cavity scan data is obtained from the experimental set up. We had repeated the experiment with the heaters heating the ETM mirror off as well as with the heaters on. The data collected is plotted together as shown in Figure 19. Here the orange line indicates the cavity scan data with the heaters off. Where as the black line indicates the cavity scan data with the heaters on. Here we can see that in both the cases frequency TEM_{00} mode is matching perfectly. But there is some frequency shift in the case of higher order modes when we heat the ETM mirror. This shift is appearing because of the change in radius of curvature of the ETM mirror. The first graph gives us information about the intensity of each mode. And the second graph gives us information about the phase change corresponding to each mode. Sharpe change in phase represents a mode. It is easier to understand the mode frequency from the phase data than from the magnitude data.

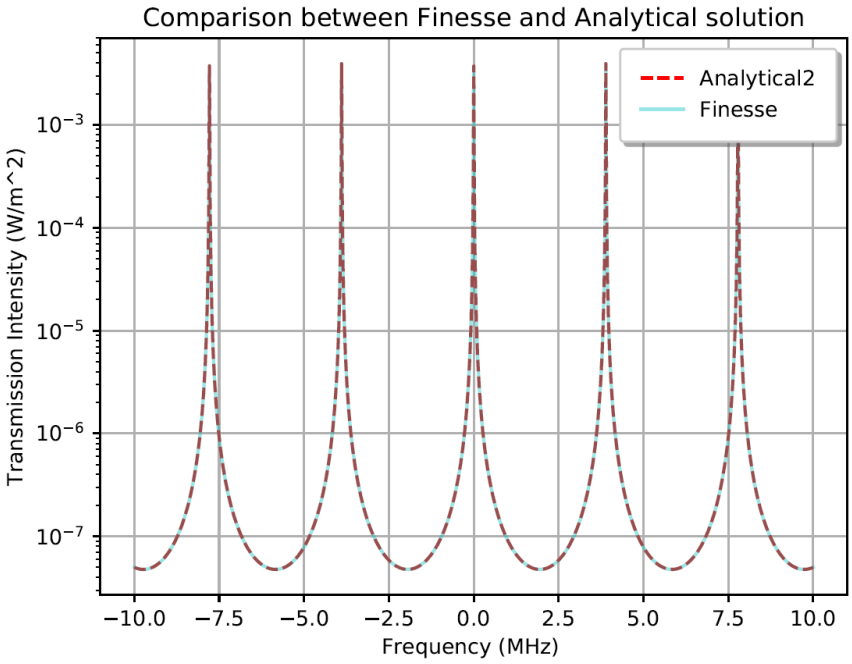

Figure 17: Graph shows the cavity scan from analytical solution developed with the help of numerical calculation as well as the cavity scan obtained from the finesse model. From the graph we can see that both of them are perfectly matching.

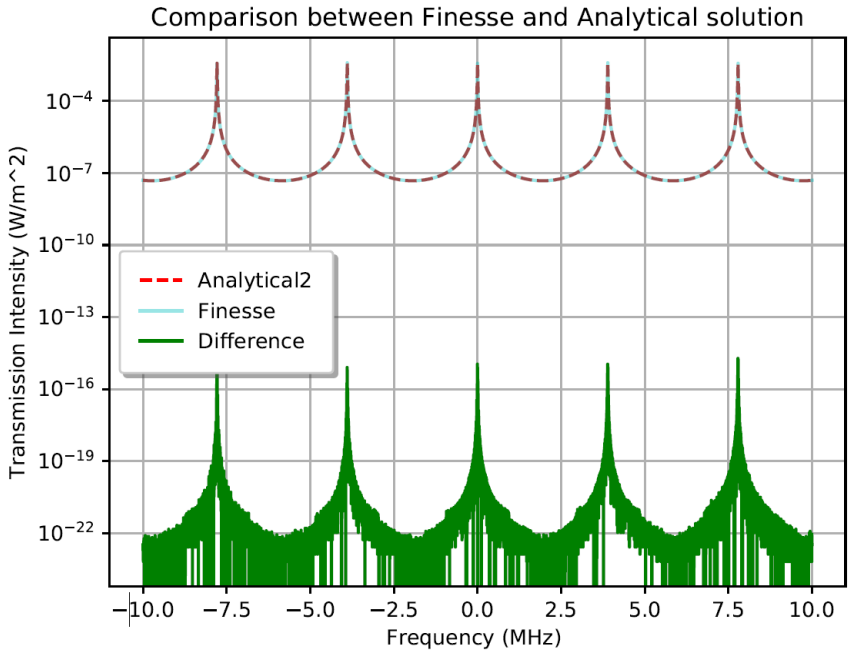

Figure 18: Graph showing the difference between the analytical solution and the finesse software solution of the cavity scan.

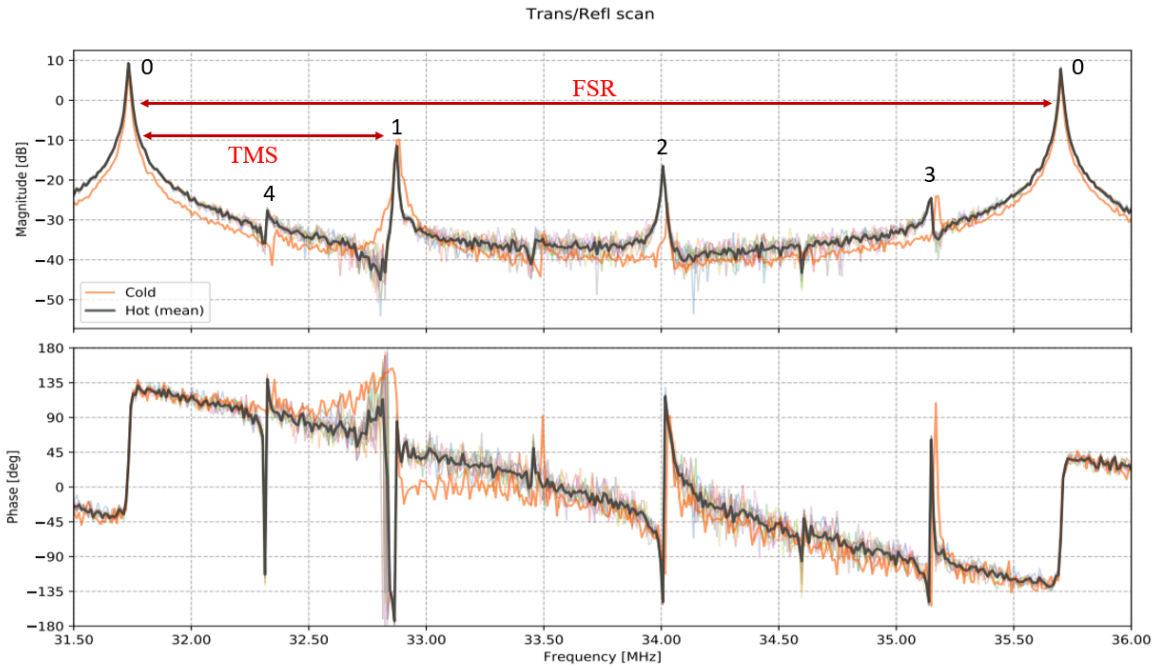

Figure 19: A plot of the experimental cavity scan data obtained with and without heating the ETM mirror.

8 Acknowledgements

First of all, I would like to thank my mentors Gautam Venugopalan, Koji Arai and Rana Adhikari for their guidance, support, encouragement and support.

I would like to thank LIGO-INDIGO scientific collaboration, LIGO 40m team and the Caltech Student-Faculty Programs office for providing the funding and support to make this dream of mine to come true.

I would like to thank the entire members of LIGO Caltech for their wonderful welcoming. Also, I would like to thank my co-mentors Jonathan Richardson, Annalisa and Terra for guiding me through this and for being so much approachable.

I would like to thank Alex Urban and Alan Weinstein for their fantastic organization of the LIGO SURF program and for cheerfully sharing lots of fun stories with me. I would like to specially thank my project partner, Sandrine Ferrans for all the helps and support.

I would also like to thank the LIGO SURF-2018 team for all the amazing experiences and memories we share together. I am giving my heart felt thanks to Larry Wallace and Michael Pedraza for all the technical support given throughout this project. I would like to thank Carolyn Peterson for amazingly scheduling all my travels and for giving me mental support at the times of crisis. I would like to thank Carol S Casey for her pleasant welcoming and guidance.

I would like to thank my parents for always supporting my dreams, for motivating me to reach heights and for their prayers. I would like to thank my grandparents for believing in

me and encouraging me.

References

[1] M. Maggiore, *"Gravitational waves"*. Oxford University Press(2008).

[2] B. P. Abbott et al, *"Observation of Gravitational Waves from a Binary Black Hole Merger"*. LIGO Scientific Collaboration and Virgo Collaboration(2016).

[3] https://www.ligo.caltech.edu/page/ligos-ifo

[4] 40m Interferometer Image https://www.ligo.org/images/faq-ifo.png

[5] G. Billingsley, H. Yamamoto, and L. Zhang, *"Characterization of Advanced LIGO Core Optics"* https://dcc.ligo.org/LIGO-P1700029

[6] Kaustubh Singhi, Koji Arai and Rana Adhikari *"Mirror Metrology using Mode Spectroscopy", LIGO-T1700195-v1*

[7] Naomi Wharton, Koji Arai and Rana Adhikari, *"Laser Mode Spectroscopy for Mirror Metrology", LIGO-T1700195-v3*

[8] Anthony E. Siegman, *"Lasers", University Science Books*

[9] K. Arai, A. Stochino, R. Adhikari, and the LIGO 40m Lab, *"Precise Measurements on Longitudinal and Transverse Mode Spacings of an Optical Cavity using an Auxiliary Laser."* https://dcc.ligo.org/LIGO-G080467

[10] OPL online course

[11] G. Vajente, *"Introduction to GW detectors."* https://dcc.ligo.org/LIGO-G1701153

[12] B. E. A. Saleh and M. C. Teich, *"Fundamentals of Photonics."*